Gait Analysis and Control of Rimless Wheel Rovers for Planetary Exploration

Dennis Schlee[1,2], Shubham Vyas[1,3], Raúl Domínguez[1], and Frank Kirchner[1,3]

Abstract—**Rimless wheeled robots are a hybrid variant of traditionally wheeled and legged robots. These hybrid systems combine the benefits of both approaches, such as power efficiency and good terrain traversability. However, the simplicity of the design of the rimless wheel has the disadvantage of limiting the flexibility of foot placement and the impacts caused on the body when navigating rigid surfaces. In this work, we focus on analyzing the effects of different gaits on the robot's center body. For that, a novel gait classification approach for a rimless wheeled system is introduced and the effects of selected gaits are evaluated in a simulation using a simplified robot model. The analysis of simulation results shows that the chosen gait has a strong effect on the vertical motion of the robot's center body.**

Index Terms—**Rimless Wheel, Micro-Rover, Gait Analysis, Vertical Motion, Drake**

I. INTRODUCTION

Autonomous wheeled rovers are a promising approach for the exploration of unknown human-hostile environments. An example of such an environment is the Martian surface, for which robotic systems like NASA's Perseverance rover [1] and the upcoming ESA's ExoMars rover [2] have been designed. A limiting factor of such wheeled rovers is that they cannot overcome steep obstacles. While legged robots have the capability of navigating in more challenging environments, they come with the disadvantage of having higher energy demands, an increased number of critical points of failure, and more complex control approaches [3].

With this trade-off in mind, robot designers have constructed hybrid systems, which pursue to combine the benefits of the two approaches. One of these hybrid variants is the rimless wheel rover, which is simple in design, efficient in power demands, and can provide better terrain traversability than an equivalent system with normal wheels.

However, the simplicity of the design of the rimless wheel has the disadvantage of limiting the flexibility of foot placement when compared to legged systems with multiple joints per leg. In comparison with wheeled systems, the main disadvantage lies in the introduction of vertical hub movement of the wheel. This vertical hub movement of each wheel often results in strong vibrations of the rover center body, especially when navigating rigid surfaces. Consequently, this leads to noisy sensor data, a reduction of efficiency on

locomotion, and faster wear of some hardware mechanisms. To tackle those limitations, we propose a gait controller that pursues the minimization of the occurring vibrations during the spoke impact phases by regulating the phase shift of each joint while applying the full system's motion command. To determine which gaits result in the minimal motion, a simulation has been set up to analyze the effects of different gaits on the vertical and the roll-pitch-yaw motion of the robot's center body.

The rimless wheel as a conceptual framework for passive-dynamic walking was introduced in [4], and such a system was comprehensively analyzed in [5]. Rimless wheels with various designs have been successfully applied in various robotic systems, including Whegs (Wheel legs) with six three-spoked rimless wheels [6] and RHex with a single arched leg on each of its six appendages [7].

Furthermore, mobile autonomous robots adapted to rimless wheel platforms have been seen in literature: In [8] the performance of planar skid-steer odometry is improved in an articulated rimless rover by combining the articulated motion model, probabilistic contact forces, and slippage estimation with inertial measurements. [9] presents a simultaneous localization and mapping (SLAM) approach that incorporates information extracted from the rover spoke interactions with the surfaces to improve the environment reconstruction process for visual approaches. Rimless wheel rovers have been studied and tested in analog environments for planetary cave exploration missions for analyzing the rover mobility features and an autonomous navigation architecture using onboard physical simulations to enhance safety [10], [11].

Given their effectiveness and simplicity, several papers regarding control strategies have been published for different rimless wheel systems: Control architectures [12] and foot placement control [13] have been developed for differential drive rovers with two rimless wheels, and a control strategy for a rimless wheel rover with unequal number of spokes on each wheel has been developed by [14]. The dynamics of rimless wheels during collisions are explored in [15]. Furthermore, three different wheel offsets on a four-wheeled rimless wheel rover were tested in [16] to find a locomotion system with the least amount of vertical motion of the robot's center body.

As described above, the development of the control architecture [12] and the foot placement control [13] have been done on a two-wheeled rimless wheel system. These works only consider one- or two-dimensional motion of the system. In this paper, we extend their work to a more complex system with four rimless wheels. Consequently, the motion

[1]DFKI GmbH - Robotics Innovation Center, Bremen, Germany. E-mail: dennis.schlee@dfki.de, shubham.vyas@dfki.de, raul.dominguez@dfki.de, frank.kirchner@dfki.de

[2]Intelligent Autonomous Systems Group at the Technical University of Darmstadt, Darmstadt, Germany.

[3]AG Robotics, Department of Mathematics and Computer Science, University of Bremen, Bremen, Germany.

around the pitch axis is introduced. Furthermore, while the locomotion system of a four-wheeled rimless wheel system found in [16] resulted in a reduction of rover bouncing, a sophisticated gait controller can be developed for an even higher reduction of vertical motion as shown in this paper. Quadrupedal gaits classification can be seen in [17] and are usually referred to in the literature as *Hildebrand*-style gait diagrams. To the best of the author's knowledge, no classification of gaits on rimless wheel systems currently exists in the literature. We also present an adapted version of the *Hildebrand*-style gait diagrams for rimless wheel rovers.

This paper is organized as follows: A system description of the hardware used is given in section II, we aim to bridge the gap between the two aforementioned research topics and introduce a novel gait classification approach for rimless wheel robots in section III. The classification of the gaits is followed by section IV, which introduces the gait controller. Following that, section V describes a simulation that analyses the effects of different gaits on the robot center body. The simulation results are then evaluated in section VI, followed by the conclusion and outlook in section VII.

II. System Description

The micro-rover Coyote II [18] is the second iteration of the Coyote rover family [19], and it has been designed to act as a scouting platform paired up with a primary rover for autonomous long-term exploration. The highly mobile rover can move on soft soil, as well as on unstructured terrain, see Fig. 1.

The rover has a boundary box size of 850 x 516 x 415 mm and a mass of 9.2 kg excluding payload. The main body is shaped in a double-decker structure, with the top and bottom layers consisting of an Arix core and aramid fiber layers. The robot is equipped with four Robodrive ILM 50x80 brushless DC motors with Harmonic Drive gearing, which produce a maximum torque of 28 Nm and a maximum rotational frequency of 50 rpm. This results in the rover having a maximum linear velocity of 0.65 m/s. The sensor fleet includes the laser range finder Hokuyo UTM-30XL, two AVT F33B stereo cameras (horizontal FoV: 118.6°), and the IMU Xsrens MTi-300 AHRS. The onboard computer is an IntelCore i7-3517UE, 1.7 GHz. The electrical power supply is provided through a lithium-ion polymer battery (44.4 V, 2.1 Ah) [20], [18].

The rover is equipped with four rimless wheels, each attached to one motor. A passive roll joint at the rear axis allows the spokes of the rimless wheel to stay in contact with the ground while the rover drives over obstacles. The rimless wheel design is based on the wheels used in the micro-rover Asguard v1 [21]. The adapted design used in Coyote II is illustrated in Fig. 2. The wheel has five equally spaced spokes, with an inter-spoke angle of $\frac{2}{5}\pi$. The spoke length is 21 cm and the height of the wheel hub during the double support stance is 18 cm. Shock-absorbing spoke tips are used to reduce physical shock during spoke impact.
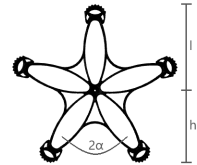

Fig. 1: Coyote II standing on fine sand [20].

Fig. 2: Illustration of the rimless wheel design used in Coyote II.

III. Gait Classification

Gait refers to the way animals move their limbs while in motion. The choice of a used gait is based on several factors, such as speed, maneuverability, and energy efficiency. The movement of each limb during a gait cycle is separated into a stance phase, where the foot is in contact with the ground, and a flight phase, where the foot is suspended in the air and moves forward. The gaits of quadrupeds have been analyzed and classified by Hildebrand [17]. His work introduced a gait diagram with which different gaits can be visually presented. Those diagrams are illustrated in Fig. 3. The y-axis denotes the individual limbs, with the following abbreviations: Left (L), right (R), front (F), and hind (H), while the x-axis represents the percentage of the gait cycle. The bars indicate the time when the foot is in the stance phase, and the horizontal area where the bar is absent indicates the time when the foot is in the flight phase.
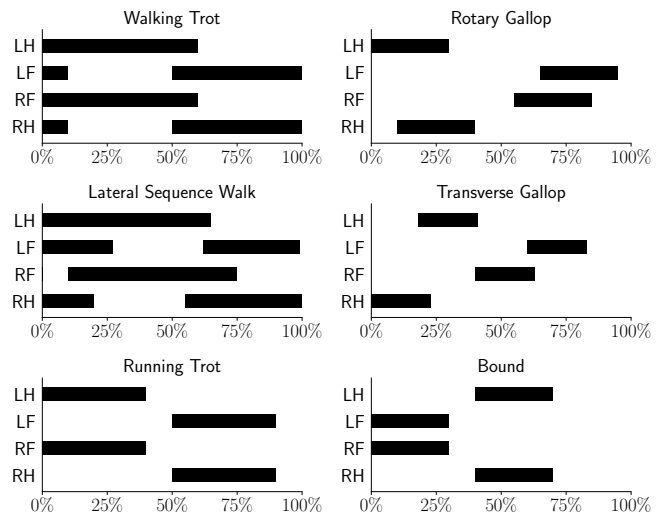

Fig. 3: Hildebrand-style gait diagrams for quadrupeds.

The means to visually present different gaits of a rimless wheel robot can be beneficial for designing a gait controller. However, directly applying the gait classification of quadrupeds to rimless wheel robots is not possible when the assumption is made, that the wheels should not have a deliberate flight phase during each gait cycle. Therefore, a novel Hildebrand-style gait diagram adapted to the rimless wheel is proposed and illustrated in Fig. 4. Similar to the work of Hildebrand, this proposed method also requires the

wheels to complete a cycle in the same length of time for a steady pattern to occur, thus assuming the robot moves forward on a level surface in an unobstructed environment. The x-axis represents the phase shift of the individual wheels relative to a reference wheel (here the left hindwheel is chosen). This phase shift can take values between zero and the inter-spoke angle 2α. With this change, the long bars indicating the contact time are substituted for markers of equal length, only indicating the moment of a new spoke contact. Quadruped gaits with the same footfall order, but with different contact times, are distilled into a single gait. Therefore, *Walking Trot* and *Running Trot* from Fig. 3 are combined into *Trot* in Fig. 4.
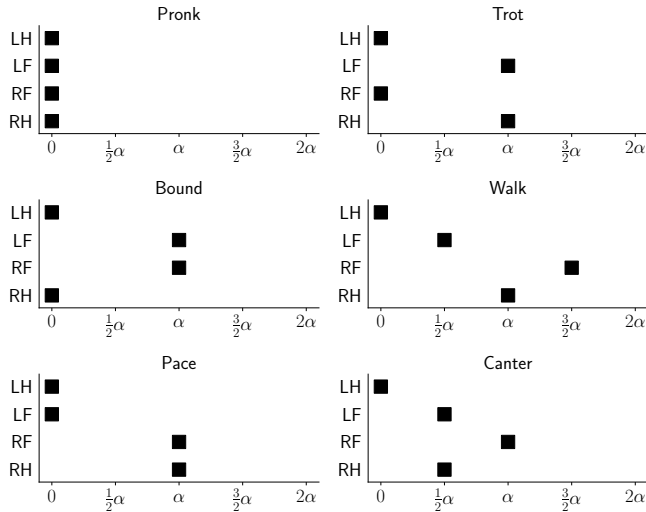

Fig. 4: Hildebrand-style gait diagrams adapted to the rimless wheel.

IV. GAIT CONTROLLER

This section introduces a gait controller for a rimless wheel rover based on the phase shift offsets of the individual wheels, as is presented in Fig. 4. Fig. 5 illustrates a framework-independent control loop diagram, incorporating the proposed gait controller within a dashed-line block and all necessary components for its functionality. The internal control flow of the proposed gait controller is depicted in Fig. 6. This control plant assumes that the gait controller controls for angular velocity commands and the contact detection occurs by tracking the joint's angular position.

The motion controller converts linear velocity commands into the physical quantity used to control the motors and then passes it to the gait controller. Together with the current state of the joints, the contact data, and a user-defined target gait, the gait controller adjusts the joint commands for the system to gradually approach the target gait. These adjusted joint commands are parsed through the joint command dispatcher to create motor commands for the motor driver, which controls the motors. The state of the motors is read out by the joint state dispatcher, which passes the information to the gait controller and the contact detector. The resulting contact data is fed back into the gait controller, completing the loop.

The proposed gait controller contains two functions: `selectTargetGait()` and `adjustJointCommand()`. Their respective pseudocode is presented in algorithm 1 and algorithm 2. The function `selectTargetGait()` compares the user input `target_gait` with a predefined configuration file containing the selectable gaits in `gait_data`. Its output, a valid target gait, is an input to the function `adjustJointCommand()` together with the angular velocity commands in `join_command_in`, the current joint angular velocity in `joint_state` and the `contact_data`. The function processes the input data and outputs adjusted angular velocity commands in `joint_command_out`, resulting in the robot gradually approaching the target gait.
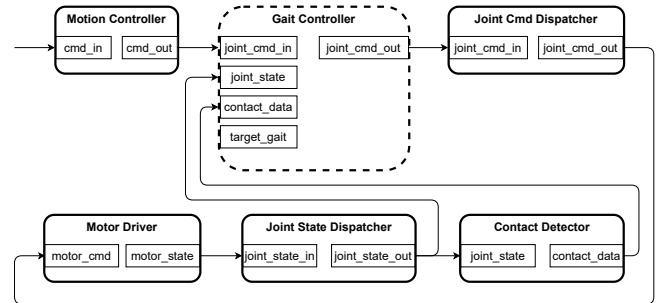

Fig. 5: A framework-independent control loop diagram, incorporating the proposed gait controller within a dashed-line block and all necessary components for its functionality.
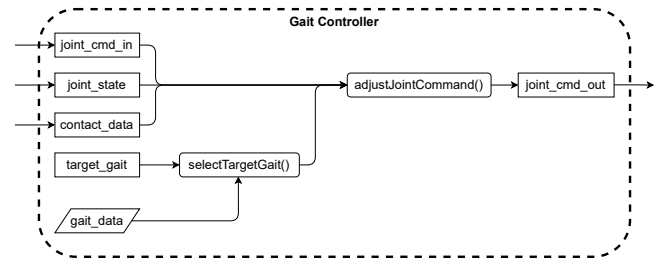

Fig. 6: Internal control flow of the proposed gait controller.

Algorithm 1: Pseudocode of the function `selectTargetGait()`.

Input: targetGait, gaitData
Output: targetPhaseShift
if *targetGait is an element of gaitData* **then**
    return *targetPhaseShift of targetGait from gaitData*
else
    return *targetPhaseShift of a default gait from gaitData*

V. GAIT ANALYSIS

A simulation has been set up to observe the effects of different gaits on the vertical motion of the robot's center body while the robot moves forward in an unobstructed

Algorithm 2: Pseudocode of the function `adjustJointCommand()`.

Input: `jointCommandIn`, `jointState`, `contactData`, `targetPhaseShift`

Output: `jointCommandOut`

if *targetPhaseShift values are not valid* **or** *jointCommandIn does not result in a forward motion of the robot* **then**
    | **return** *jointCommandIn*

initialize `jointCommandOut`

foreach *wheel* **do**
    if *new contact for the wheel has occured* **then**
        | read `angularPosAtContact`

save `contactData` for next iteration

if *new contact occurred for all wheels* **then**
    | `gaitDetected` ⟵ true

if *gaitDetected* **then**
    calculate `currentPhaseShift` of each wheel by comparing `currentAngularPos` and `angularPosAtContact`
    adjust velocity commands based on the difference between `currentPhaseShift` and `targetPhaseShift`
    write adjusted velocity commands into `jointCommandOut`
else
    | **return** *previousJointCommandOut*

`previousJointCommandOut` ⟵ `jointCommandOut`
return *jointCommandOut*
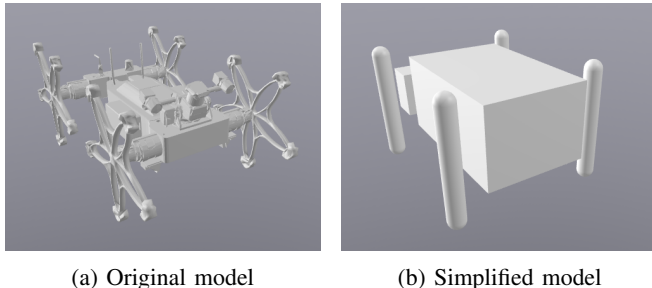

(a) Original model   (b) Simplified model

Fig. 7: Comparison of the original and the used simplified model of Coyote II for the gait analysis simulation.

environment. Furthermore, the analysis also includes the effects of the used gait on the roll-pitch-yaw motion and the phase portrait of the z-axis. The analyzed gaits are the ones presented in Fig. 4: Pronk, Bound, Pace, Trot, Walk, and Canter. The simulation uses a simplified geometry of the robot, where the rimless wheels attached to revolute joints have been substituted for elongated capsules acting as legs, attached to vertical prismatic joints, resulting in the model staying in place during the simulation. This simplified geometry seen in Fig. 7 results in a reduction of complexity of the simulated model without a loss of relevant information. The legs are actuated in a sinusoidal pattern, where each leg

has an offset as described in the aforementioned diagram. The actuation length of the prismatic joints is equal to the height difference of the rimless wheel hub during the double support stance and the spoke length (see Fig. 2). To ensure accurate results, the actuators are enabled after the model has settled after spawning. The simulation has been done using Drake [22].

VI. EVALUATION

This section evaluates the results of the simulation described in section V of the six selected gaits Pronk, Bound, Pace, Trot, Walk, and Canter. The vertical motion and the roll-pitch-yaw motion of the robot center body during the simulation of the six selected gaits are illustrated in Fig. 8 and the peak-to-peak amplitude values during a wave period are compared in Table I. Fig. 9 displays the phase portraits of the z-axis of the robot center body of all the six selected gaits.

TABLE I: Comparison of the peak-to-peak amplitude values of the vertical motion and the roll-pitch-yaw motion during a wave period for the selected gaits.

Gait	*Vertical motion [mm]*	*Roll motion [deg]*	*Pitch motion [deg]*	*Yaw motion [deg]*
Pronk	28.2	**0.0**	**0.0**	**0.0**
Bound	28.2	**0.0**	6.1	**0.0**
Pace	**1.7**	6.6	0.1	**0.0**
Trot	**1.7**	6.2	0.1	2.7
Walk	1.8	6.9	0.4	1.9
Canter	20.0	5.0	3.1	1.4

A. Vertical Motion

Using the gaits Pace (1.7 mm) and Trot (1.7 mm) results in the least vertical motion of the robot center body, closely followed by Walk (1.8 mm). The vertical motion while using Canter (20.0 mm), Pronk (28.2 mm), and Bound (28.2 mm) is considerably higher.

B. Roll Motion

The gaits Pronk (0.0 deg) and Bound (0.0 deg) do not have a roll motion. These results are expected, considering the spoke contact order of both of these gaits do not introduce a roll motion in the robot. The remaining four gaits have a roll motion, with values close to one another: Canter (5.0 deg), Trot (6.2 deg), Pace (6.6 deg), Walk (6.9 deg).

C. Pitch Motion

The gait Pronk (0.0 deg) does not have a pitch motion. Pace (0.1 deg), Trot (0.1 deg), and Walk (0.4 deg) follow closely with a negligible, but non-zero pitch motion. The spoke contact order of those four gaits should not introduce a pitch motion in the robot. The reason why the pitch motion is still non-zero is due to the unequal mass distribution, resulting in the center of mass lying in the front half of the robot. The gait Canter (3.1 deg) introduces a small pitch motion, while the value of Bound (6.1 deg) is nearly double the amount.
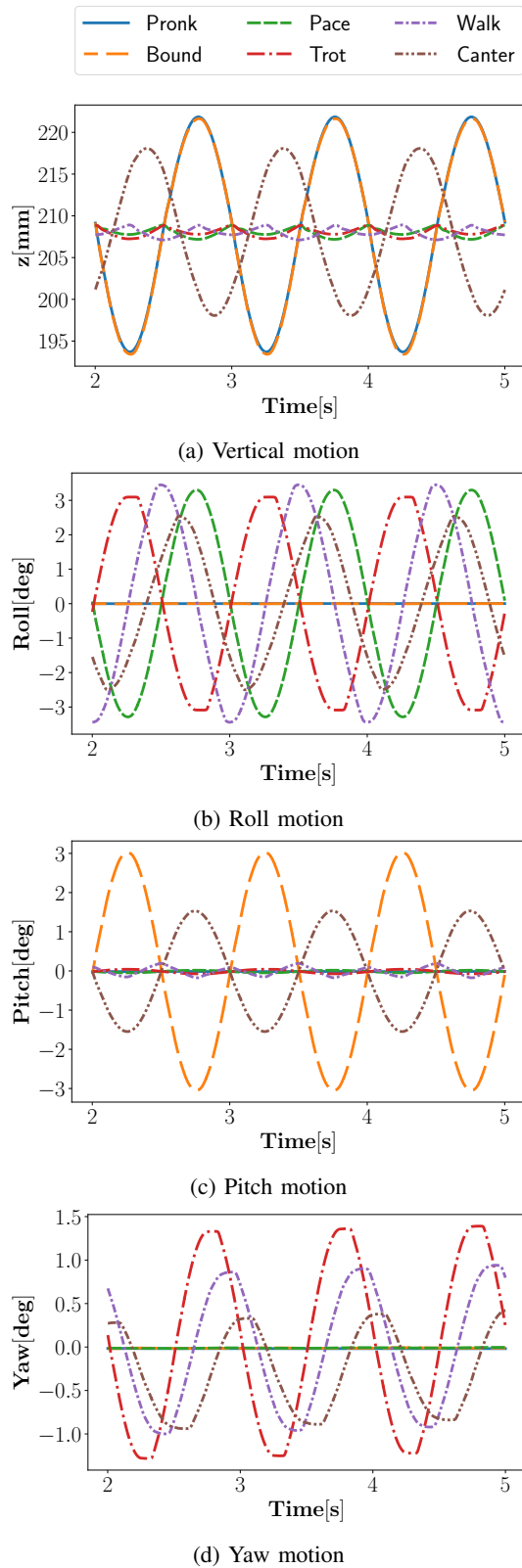
(a) Vertical motion

(b) Roll motion

(c) Pitch motion

(d) Yaw motion

Fig. 8: Comparison of the vertical motion and the roll-pitch-yaw motion of the robot center body during the simulation of the six selected gaits.
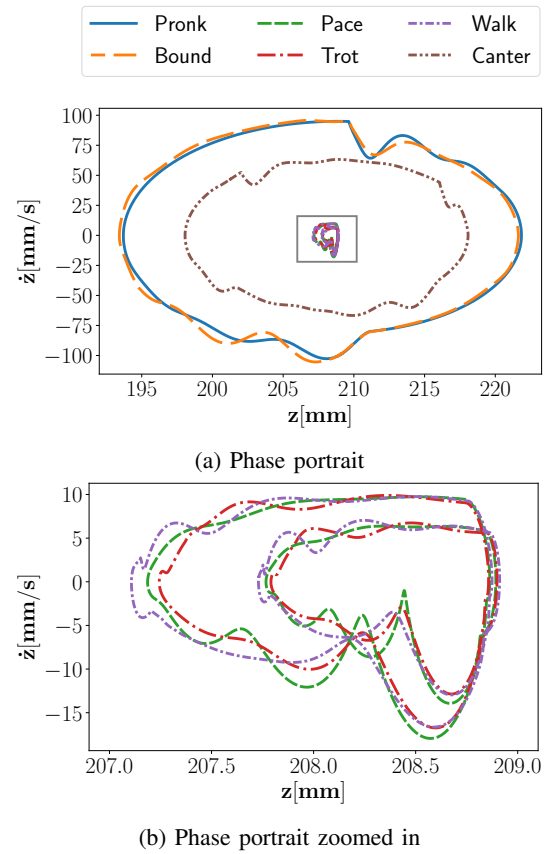

(a) Phase portrait

(b) Phase portrait zoomed in

Fig. 9: Comparison of the phase portraits of the z-axis of the robot center body during the simulation of the six selected gaits.

D. Yaw Motion

The gaits Pronk (0.0 deg), Bound (0.0 deg), and Pace (0.0 deg) do not introduce a yaw motion, as is expected from the spoke contact order. Canter (1.4 deg), Walk (1.9 deg), and Trot (2.7 deg) introduce a small yaw motion. A noteworthy detail in the plot is that the average yaw motion of all gaits except for Pronk rises over time. The unequal mass distribution, combined with the unsynchronized spoke contact order of the five referenced gaits, results in the model slowly moving away from the initial position with a rising rotation around the z-axis. The rising average yaw motion of some gaits is presumed to be the result of the simplification of the robot model and is not expected to occur on a system equipped with four rimless wheels.

E. Phase Portrait

The gaits Pronk and Bound result in the largest and nearly identical phase portraits, followed by Canter with a slightly smaller phase portrait with a similar shape. Pace, Trot, and Walk result in considerably smaller phase portraits. Furthermore, the phase portraits of the latter three gaits result in a significantly different shape. The results of the sizes of the individual phase portraits are congruent with the results of the vertical motion.

VII. CONCLUSION AND OUTLOOK

This paper introduces a novel gait classification approach for rimless wheel rover, based on the phase shift offsets of the individual wheels. On this basis, a gait controller is presented that utilizes the phase shift approach to control the gait of a rimless wheel rover. Consequently, a simulation is presented that analyses and compares the effects of six selected gaits on the robot center body on a simplified robot model. Evaluating the simulation results show, that the gaits Pace, Trot and Walk have the least effect on the vertical motion of the robot center body. The two gaits Pronk and Bound do not introduce a roll motion. When the goal is to minimize the pitch motion, the gaits Pronk, Pace, Trot, and Walk are all appropriate choices. For minimizing the yaw motion, the three gaits Pronk, Bound and Pace are the most suitable options. The simulation results presented in this paper can be applied to minimize the overall motion experienced by a rimless wheel rover during navigation on a rigid surface. Consequently, this can enhance locomotion efficiency, improve sensor data, and extend mission duration.

Building on the findings of this paper, the future work will focus on simulation-based optimization to find a gait with the least vertical motion of the robot center body. Finally, the gait controller and a suitable contact detection method are to be implemented on the autonomous navigation stack of the Coyote II rover, to validate the simulation results on the hardware.

REFERENCES

[1] K. A. Farley, K. H. Williford, K. M. Stack, R. Bhartia, A. Chen, M. de la Torre, K. Hand, Y. Goreva, C. D. Herd, R. Hueso, *et al.*, "Mars 2020 mission overview," *Space Science Reviews*, vol. 216, pp. 1–41, 2020.

[2] J. L. Vago, F. Westall, A. J. Coates, R. Jaumann, O. Korablev, V. Ciarletti, I. Mitrofanov, J.-L. Josset, M. C. De Sanctis, J.-P. Bibring, *et al.*, "Habitability on early mars and the search for biosignatures with the exomars rover," *Astrobiology*, vol. 17, no. 6-7, pp. 471–510, 2017.

[3] J. Liu, M. Tan, and X. Zhao, "Legged robots—an overview," *Transactions of the Institute of Measurement and Control*, vol. 29, no. 2, pp. 185–202, 2007.

[4] T. McGeer, "Passive dynamic walking," *The international journal of robotics research*, vol. 9, no. 2, pp. 62–82, 1990.

[5] M. J. Coleman, *A stability study of a three-dimensional passive-dynamic model of human gait*. Cornell University, 1998.

[6] R. D. Quinn, J. T. Offi, D. A. Kingsley, and R. E. Ritzmann, "Improved mobility through abstracted biological principles," in *IEEE/RSJ International Conference on Intelligent Robots and Systems*, vol. 3, pp. 2652–2657, IEEE, 2002.

[7] G. C. Haynes and A. A. Rizzi, "Gaits and gait transitions for legged robots," in *Proceedings 2006 IEEE International Conference on Robotics and Automation, 2006. ICRA 2006.*, pp. 1117–1122, IEEE, 2006.

[8] J. Hidalgo-Carrio, A. Babu, and F. Kirchner, "Static forces weighted jacobian motion models for improved odometry," in *2014 IEEE/RSJ International Conference on Intelligent Robots and Systems*, pp. 169–175, IEEE, 2014.

[9] J. Schwendner, S. Joyeux, and F. Kirchner, "Using Embodied Data for Localization and Mapping," *Journal of Field Robotics*, vol. 31, pp. 263–295, Mar. 2014.

[10] R. Domínguez, S. Arnold, C. Hertzberg, and A. Böckmann, "Internal simulation for autonomous robot exploration of lava tubes," in *Proceedings of the 15th International Conference on Informatics in Control, Automation and Robotics*, vol. 2, pp. 144–155, 2018.

[11] R. U. Sonsalla, S. Planthaber, R. Dominguez, A. Dettmann, F. Cordes, B. Huelsen, C. Schulz, P. Schoeberl, S. Kasperski, H. Wiedemann, and F. Kirchner, "Towards a semi-autonomous robotic exploration of a lunar skylight cavity," in *2022 IEEE Aerospace Conference (AERO)*, pp. 1–20, 2022.

[12] K. Shankar and J. W. Burdick, "Motion planning and control for a tethered, rimless wheel differential drive vehicle," in *2013 IEEE/RSJ International Conference on Intelligent Robots and Systems*, pp. 4829–4836, IEEE, 2013.

[13] S. Sanchez and P. A. Bhounsule, "Design, modeling, and control of a differential drive rimless wheel that can move straight and turn," *Automation*, vol. 2, no. 3, pp. 98–115, 2021.

[14] M. Sun, S. Li, X. Liu, R. Zhang, and G. Zong, "Tripod gait planning of a rimless-wheeled robot with changeable spokes," in *2009 IEEE International Conference on Robotics and Biomimetics (ROBIO)*, pp. 1715–1720, IEEE, 2009.

[15] Y. Iwatani, "Dynamics of rimless wheel robots during collision," *SICE Journal of Control, Measurement, and System Integration*, vol. 15, no. 1, pp. 1–9, 2022.

[16] A. Babu, S. Joyeux, J. Schwendner, F. Grimminger, and D. R. I. Center, "Effects of wheel synchronisation for the hybrid leg-wheel robot asguard," in *Proceedings of International Symposium on Artificial Intelligence, Robotics and Automation in Space (iSAIRAS-10), Sapporo*, 2010.

[17] M. Hildebrand, "The quadrupedal gaits of vertebrates," *BioScience*, vol. 39, no. 11, p. 766, 1989.

[18] R. U. Sonsalla, Y. Nevatia, M. Fritsche, J. B. Akpo, J. Gancet, F. Kirchner, and D. R. I. Center, "Design of a high mobile micro rover within a dual rover configuration for autonomous operations," in *Proc. Int. Symp. Artif. Intell., Robot. Autom. Space*, p. 8, 2014.

[19] R. Sonsalla, J. Akpo, and F. Kirchner, "Coyote III: Development of a modular and highly mobile micro rover," in *Advanced Space Technologies in Robotics and Automation (ASTRA-2015)*, May 2015.

[20] DFKI-RIC, "Coyote II." https://robotik.dfki-bremen.de/en/research/robot-systems/coyote-ii. Accessed: 2023-12-04.

[21] M. Eich, F. Grimminger, S. Bosse, D. Spenneberg, and F. Kirchner, "Asguard: A hybrid-wheel security and sar-robot using bio-inspired locomotion for rough terrain," *Proceedings ROBIO*, vol. 20082008, pp. 774–779, 2008.

[22] R. Tedrake and the Drake Development Team, "Drake: Model-based design and verification for robotics," 2019.